ELSEVIER

Nuclear Physics A 637 (1998) 469–490

NUCLEAR PHYSICS A

High-spin isomers in ^{211}Po and related structures in ^{210}Po and ^{212}Po

T.R. McGoram [a], G.D. Dracoulis [a], A.P. Byrne [a,1], A.R. Poletti [b], S. Bayer [a]

[a] *Department of Nuclear Physics, RSPhysSE, The Australian National University, Canberra, ACT 0200, Australia*

[b] *Department of Physics, University of Auckland, Private Bag 92019, Auckland, New Zealand*

Received 17 April 1998; accepted 6 May 1998

Abstract

High-spin states in ^{211}Po have been populated through the incomplete fusion reactions ^{208}Pb(^{9}Be,$\alpha 2n$) and ^{208}Pb(^{7}Li,$p3n$). The yrast sequence decaying to the τ_m = 36.4 s isomer in ^{211}Po has been established to a spin of $(43/2^+)$ at an excitation energy of 4873 keV. Two other isomeric levels have been identified, with mean lives of 350(30) ns and 4(1) μs at excitation energies of 2135.7 keV and 4873.3 keV, respectively. Relationships between the structure of high-spin states in ^{211}Po and those previously identified in ^{210}Po and ^{212}Po are discussed. © 1998 Elsevier Science B.V.

Keywords: NUCLEAR REACTIONS ^{208}Pb(^{9}Be,$\alpha 2n$), E = 50 MeV; measured $\alpha\gamma\gamma(t)$, $\alpha\gamma(t)$, E_γ; ^{208}Pb(^{7}Li, $p3n$), E = 56 MeV; measured $\gamma\gamma(t)$, E_γ. ^{211}Po deduced high-spin levels, isomer $T_{1/2}$, reduced transition probabilities. Enriched targets, pulsed-beam, Compton suppressed Ge detectors.
NUCLEAR STRUCTURE ^{210}Po, ^{211}Po, ^{212}Po; calculated levels, J, π, $B(\lambda)$. Semi-empirical shell model. Yrast configurations. Residual interactions.

1. Introduction

The high-spin properties of polonium isotopes at or near the N = 126 closed neutron shell provide a stringent test of the predictions of the shell model in the trans-lead region. The energies of excited states in $^{210}_{84}Po_{126}$ and $^{211}_{84}Po_{127}$ enable residual interaction energies to be determined and provide an opportunity to study the interaction of simple

[1] Joint appointment with the Department of Physics, The Faculties, The Australian National University.

PII S0375-9474(98)00227-9

valence configurations with excitations of the ^{208}Pb core. Importantly, the configurations and properties of core-excited states in ^{210}Po and ^{211}Po may provide information on less accessible high-spin configurations present in the heavier polonium isotopes, in particular the long-lived α-decaying isomers in both ^{211}Po and ^{212}Po, each of which has been the subject of considerable experimental and theoretical effort.

However, the population of ^{210}Po, ^{211}Po and ^{212}Po at high spin via conventional (HI,xn) reactions is problematic as they are relatively neutron-rich nuclei. For the lighter isotopes, the obvious ^{208}Pb(α, xn) reactions are limited to a spin input of $\sim$ 12–16$\hbar$, inadequate for the substantial population of core-excited states, which are likely to enter the yrast sequence in ^{211}Po with spin $37/2^+$ at $\sim$ 4200 keV. An alternative reaction mechanism used with recent success in the rare-earth region [1] is that labelled 'incomplete fusion' or 'massive transfer' [2], in which fragmentation of the beam particle at the nuclear surface is followed by fusion of one fragment and emission of the remaining fragment with an energy corresponding to preservation of the beam velocity [3]. The principal advantage of such a reaction is access to equivalent beams of neutron-rich projectiles, such as ^{5}He following breakup of the ^{9}Be beam used in the present experiments. The cross-sections for the incomplete fusion reactions ^{208}Pb(^{9}Be,$\alpha 2n$)^{211}Po and ^{208}Pb(^{9}Be,$\alpha 2n$)^{211}Po^m at a beam energy of 50 MeV have been recently measured by Dasgupta et al. [4] as 15.4% and 8.7% of the total fusion cross-section, respectively.

In the ^{7}Li induced reaction, it is not clear whether the incomplete fusion or fusion-evaporation mechanism predominates in the production of the polonium isotopes. Nonetheless, the higher spin input of this reaction complemented the isotope-identification properties (outlined in [2]) of the ^{9}Be induced reaction.

The only previous in-beam study of ^{211}Po is that of Fant et al. [5] who used the reaction ^{208}Pb(α, n) at energies of 18–20.6 MeV, to establish the yrast structure up to the τ_m = 36.4 s (mean life) isomer at 1463 keV. The aim of the present work was the population of states above this, and the identification of core-excited states and their decay to known levels in this nucleus.

2. Experimental procedures

Excited states of ^{211}Po were populated with the ^{208}Pb(^{9}Be,α2n) and ^{208}Pb(^{7}Li,p3n) reactions using beams provided by the ANU 14UD Pelletron. For each reaction isotopically enriched ^{208}Pb foils were used. Several measurements were performed using each reaction and the different experimental conditions are summarised in Table 1.

2.1. Gamma-ray measurements

Gamma-rays were detected in the CAESAR array [7], which in its basic configuration, consists of six Compton suppressed HPGe detectors, at angles of $\pm 48°$, $\pm 97°$ and $\pm 145°$ to the beam axis. For the ^{9}Be induced reactions, the selection of particle–γ and particle–γ–γ coincidences was provided by the ANU Particle Detector Ball [8], an array of

Table 1
Summary of measurements performed on ^{211}Po

Experiment	Beam	Energy	Pulsing	Target	Enrichment
α–γ coincidences γ-ray singles	^{9}Be	45, 50, 55, 60 MeV	DC	3.3 mg/cm^2	99% ^{208}Pb
α–γ–γ–t γ-ray singles	^{9}Be	50 MeV	DC	2.3 mg/cm^2	98% ^{208}Pb
γ–γ–t γ-ray singles	^{7}Li	56 MeV	1 ns pulses, 856 ns separation	2.3 mg/cm^2	98% ^{208}Pb

14 phoswich detectors covering 85% of 4π in close geometry about the target. The phoswich detectors were grouped into three 'rings'; a forward ring of six detectors covering angles from 20–60° with respect to the beam axis, a middle ring covering 60–100° and a backward ring at angles 100–140°. The forward detectors were shielded with a 45 mg/cm^2 aluminium foil, to remove scattered beam particles. The hardware-set particle–γ time condition allowed the detection of either individual γ-rays or γ–γ coincidences occurring up to 856 ns after the detection of a charged particle. Alpha–$\gamma(t)$ measurements were conducted at beam energies of 45, 50, 55 and 60 MeV, resulting in 64×10^6 coincidence events. A total of 73×10^6 α–γ–$\gamma(t)$ events were collected at a beam energy of 50 MeV. The population of ^{211}Po at this energy was approximately 20% that of ^{213}Rn, the most prolific reaction product, produced via the $4n$ channel.

High-spin states in ^{211}Po were also produced in the ^{208}Pb(^{7}Li,p3n) reaction channel as a byproduct of a study [9] aimed primarily at the $5n$ product ^{210}At, and with a population of $\sim$10% relative to this nucleus at a beam energy of 56 MeV. The ^{7}Li beam consisted of 1 ns pulses separated by 856 ns. A total of 92×10^6 coincidence events were recorded in this measurement, and no charged particle channel selection was employed. The measurement of lifetimes greater than 1 μs were established following population of ^{211}Po with a 48 MeV ^{7}Li beam chopped with an on/off ratio of 11 μs/86 μs, during the study detailed in [9].

2.2. Angular distribution measurements

Analysis of the γ-ray spectra recorded in the six detectors of the CAESAR array provided three detection angles for the angular distribution measurement, and fits to the Legendre expansion $W(\theta) = A_0[1 + a_2P_2(\cos\theta)]$ gave the coefficient a_2 and the intensity, A_0.

2.3. Data reduction

2.3.1. α–$\gamma(t)$

For each bombarding energy, two matrices of E_γ vs. time (with respect to detection of the α-particle) were constructed. One matrix required the detection of an α-particle

in the forward ring of the detector ball, while the other required detection of the α-particle in either the middle or rear detector rings. Subsequent projection onto the E_γ-axis allowed the extraction of the intensity of any individual γ-ray associated with an α-particle observed in a particular detector ring.

2.3.2. α–γ–$\gamma(t)$

The event mode data were sorted into γ–γ matrices with various relative time conditions. The basic coincidence information was extracted from a 'wide prompt' matrix, consisting of pairs of γ-rays in coincidence with α-particles and detected within ± 140 ns of each other. To identify transitions associated with the population or decay of isomers, a 'long earlies' matrix containing γ-ray events detected 180–800 ns before the gating transition was created. Its transpose provided a 'long delayed' matrix. Similarly, 'short earlies' and 'short delayed' matrices with relative times between 35–150 ns selected transitions separated by isomers with mean lives in the tens of nanoseconds region.

2.3.3. γ–$\gamma(t)$

The pulsed beam used in the ^{208}Pb(^{7}Li,p3n) reaction allowed the classification of events according to their time relationship with the beam pulse. An out-of-beam γ–γ matrix was constructed, containing events detected between 300–800 ns after each beam pulse, and within 140 ns of each other. Other γ–γ matrices were created without restriction on the time relationship with the beam pulses, but with 'wide prompt', 'long early' and delayed requirements.

2.3.4. γ–γ *time difference*

Lifetimes of the order of 1 μs or less were extracted from the time differences between transitions. The event-mode data were sorted into a three-dimensional matrix, with γ-ray energies on the x- and y-axes and time differences on the z-axis. Gates placed on populating and depopulating transitions allowed the projection (after appropriate background subtraction) of the associated time difference spectrum, to obtain the decay curve of the intermediate isomeric state.

2.3.5. γ-*time*

The measurement of lifetimes greater than 1 μs was determined using the chopped ^{7}Li beam at 48 MeV. Two-dimensional matrices of γ-ray energies against time were constructed after matching of the individual times and energies of each γ-ray detector, from which background subtracted time spectra for each transition could be generated.

3. Results

The particle-gated γ-ray singles spectrum obtained in the ^{9}Be induced reaction at 50 MeV is shown in Fig. 1, with the main products indicated. The effectiveness of the

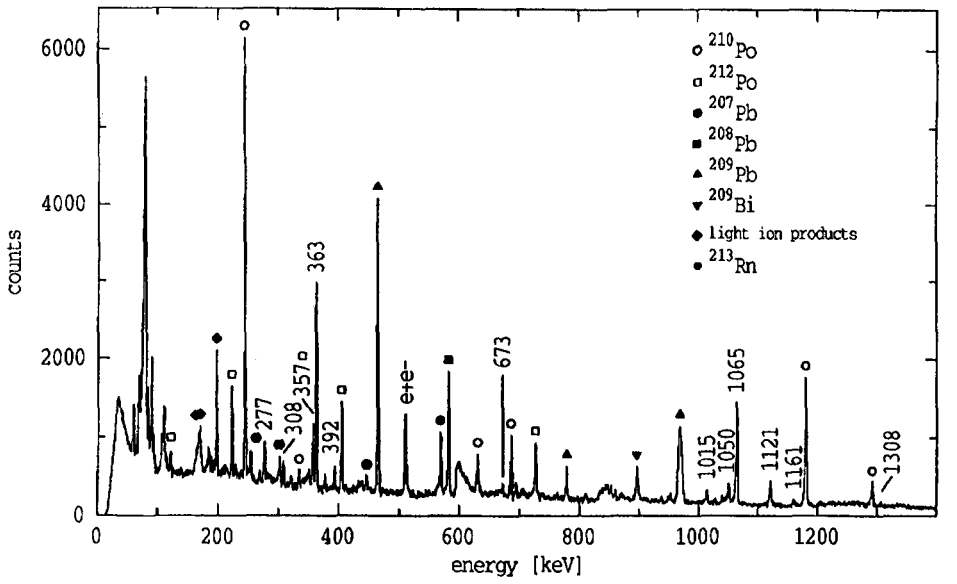

Fig. 1. Particle-gated singles spectrum for the ^{9}Be induced reaction. Gamma-rays shown are in prompt coincidence with emitted particles, leading to a reduction of intensity for transitions directly de-exciting isomers.

particle gating is demonstrated by the almost complete suppression of the ^{213}Rn lines resulting from the $4n$ reaction.

The level scheme for ^{211}Po deduced from our work is shown in Fig. 2. Table 2 lists the properties of all electromagnetic transitions assigned to ^{211}Po observed in this work, and where there is overlap with the work of Fant et al. we confirm their results. (This earlier study identified many transitions decaying from low-spin states either unobserved or weakly observed in this work, consistent with the lower spin input of the ^{208}Pb(α,n) reaction.) Newly assigned transitions are all those decaying to the τ_m = 36 s, J^π = $(25/2^+)$ α-decaying isomer, and all but four of those decaying to the $17/2^+$ state at 1427.9 keV. Relative intensities were deduced from coincidence spectra where transitions were not resolved in singles.

3.1. Assignment of transitions to ^{211}Po

The long lifetime of the α-decaying isomer effectively decouples the decay of states with spins greater than $25/2^+$ from known transitions in this nucleus, preventing a direct assignment with delayed coincidence techniques. Instead we exploit a feature recently used [1] as a channel-selection technique in similar reactions, to associate transitions in coincidence with polonium x-rays with mass 211. The reaction mechanism and experimental methods are discussed in Ref. [2].

Briefly, the ratio of γ-ray yields in coincidence with α-particles detected in the forward phoswich detector ring to those detected in the middle or rear rings displays a correlation with the number of neutrons emitted from the residual nucleus; the ratio is

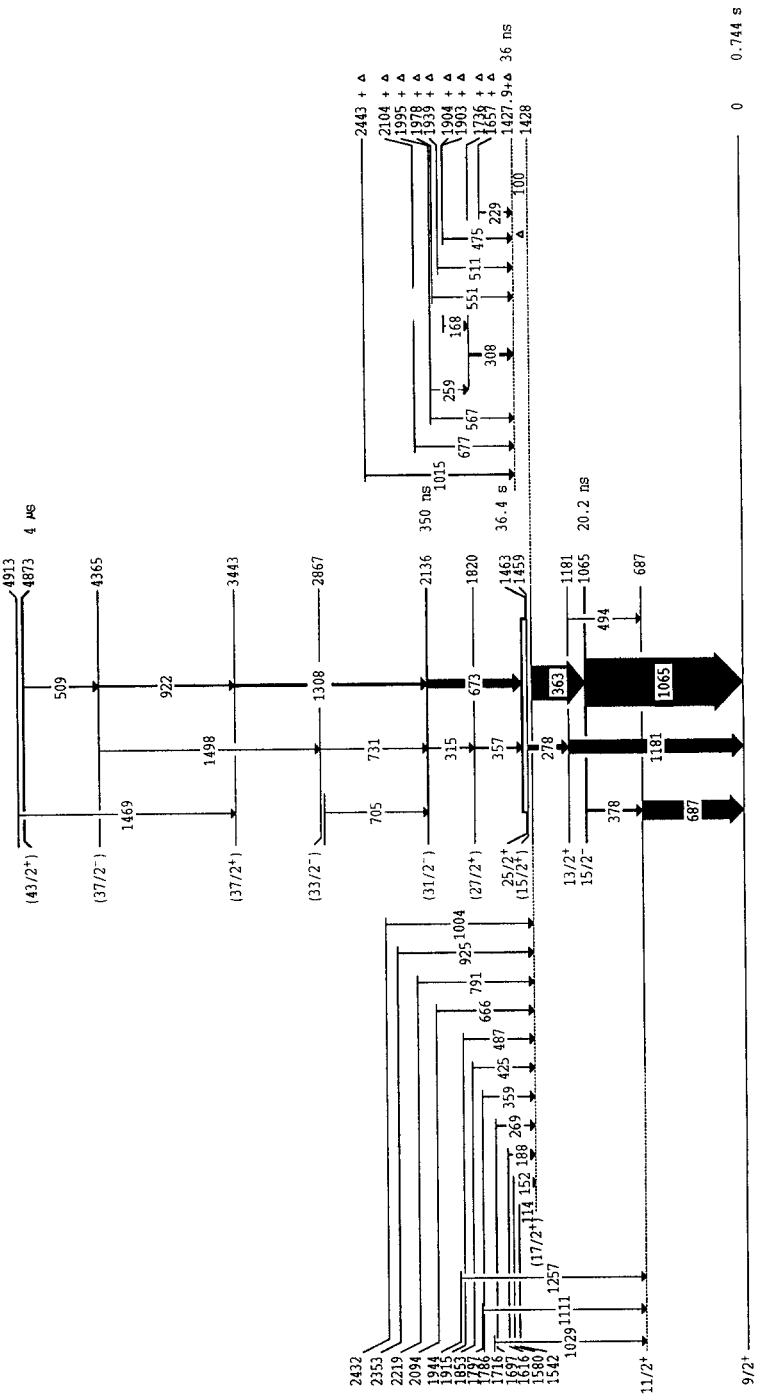

Fig. 2. Partial level scheme for ^{211}Po.

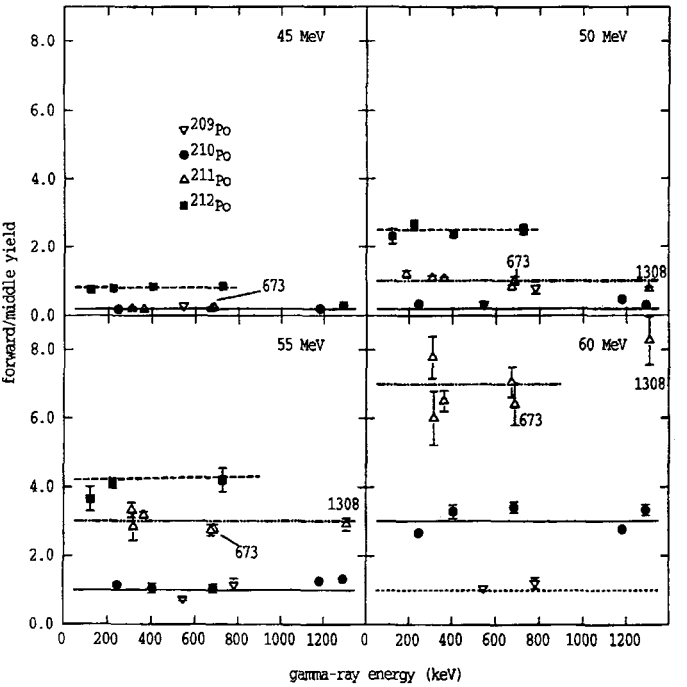

Fig. 3. Forward/middle gated intensity ratios for selected transitions in polonium isotopes.

higher the fewer the number of neutrons which are emitted, and furthermore, the ratio for a particular isotope increases sharply with the bombarding energy.

These trends are clearly visible in Fig. 3, which display the forward/middle yield ratios for the 672.7 and 1307.5 keV transitions, which we assign to states above the α-decaying isomer, together with known lines from ^{209}Po, ^{210}Po, ^{211}Po and ^{212}Po. (These were the only transitions of those we place above the α-decaying isomer with no known contaminant lines.) In the present experiments, no useful α–γ coincident yield was detected in the rear detector ring at 55 and 60 MeV bombarding energies, hence for simplicity only forward/middle ratios are shown at each energy. The clear separation of the ratios for isotopes with differing neutron number allows the assignment of the 672.7 and 1307.5 keV transitions to ^{211}Po. Their specific placement in the decay scheme is the subject of Section 3.3.

It should be noted that a quantitative understanding of Fig. 3 is complicated by several factors, such as the shielding of the forward ring of the detector ball from scattered beam by aluminium absorbers, with the resultant uncertainty in efficiency for low energy α-particles which strike the forward detectors. The absence of a recorded total energy signal and the low granularity of the particle detectors also limit a full evaluation of the reaction mechanism. Nonetheless, while our results are qualitative in nature only, they appear sufficient as a means of channel selection and thus for the assignment of isolated transitions to particular nuclei.

Table 2
Properties of transitions observed in ^{211}Po. Energies, intensities, angular distributions and initial and final energies, spins and parities of transitions assigned to ^{211}Po

E_γ	I_γ	A_2/A_0	E_i	E_f	J_i^π	J_f^π
114.0	22(4)[a]		1541.9	1427.9		$(17/2^+)$
152.1	3(1)[a]		1580.0	1427.9		$(17/2^+)$
168.3	2(1)[a]		1904.3+Δ	1736.0+Δ		$23/2^+$
187.8	35(5)	−0.11(13)	1615.7	1427.9		$(17/2^+)$
192.8	50(13)	0.26(10)	1578.0	1385.2	$(1/2^-)$	$1/2$
229.0	18(3)[a]		1656.9+Δ	1427.9+Δ		$(21/2^+)$
248.8	⩽ 2		1409.4	1160.6		$(9/2^+)$
258.9	6(1)[a]		1994.9	1736.0+Δ		$23/2^+$
268.8	18(3)[a]		1696.7	1427.9		$(17/2^+)$
276.0	⩽ 2		1436.6	1160.6		$(9/2^+)$
277.5	97(10)[a]		1458.6	1181.4	$(15/2^+)$	$13/2^+$
285.4	26(8)		1407.4	1122.0		$7/2^+$
287.7	43(12)		1409.7	1122.0		$7/2^+$
308.1	61(10)	−0.14(11)	1736.0+Δ	1427.9+Δ	$23/2^+$	$(21/2^+)$
315.4	20(3)	0.03(18)	2135.7	1820.3	$(31/2^-)$	$(27/2^+)$
334.3	47(5)		1385.2	1050.9	$1/2$	$5/2^+$
356.6	⩽ 2		1517.2	1160.6		$(9/2^+)$
357.3	49(5)[a]		1820.3	1463.0	$(27/2^+)$	$25/2^+$
358.5	25(4)[a]		1786.4	1427.9		$(17/2^+)$
363.0	705(18)	−0.14(3)	1427.9	1064.9	$(17/2^+)$	$15/2^-$
377.6	46(3)	0.07(13)	1064.9	686.9	$15/2^-$	
386.5	34(6)		1508.5	1122.0		$7/2^+$
392.1	104(6)	0.25(9)	1443.0	1050.9	$(1/2^+)$	$5/2^+$
424.7	10(1)[a]		1852.6	1427.9		$(17/2^+)$
475.0	25(5)[a]		1902.9+Δ	1427.9+Δ		$(21/2^+)$
486.9	20(5)[a]		1914.8	1427.9		$(17/2^+)$
494.2	14(3)		1181.4	686.9	$13/2^+$	
508.6	23(3)[a]		4873.3	4364.7	$(43/2^+)$	$(37/2^-)$
511.3	11(2)[a]		1939.2+Δ	1427.9+Δ		$(21/2^+)$
516.0	17(5)[a]		1638.0	1122.0		$7/2^+$
534.2	⩽ 2		1584.5	1050.8		
550.5	12(2)[a]		1978.4+Δ	1427.9+Δ		$(21/2^+)$
561.5	⩽ 2		1612.3	1050.8		
563.7	⩽ 2		1614.5	1050.8		
567.1	13(2)[a]		1995.0+Δ	1427.9+Δ		$(21/2^+)$
576.5	5(2)[a]		3443.2	2886.6		
645.7	⩽ 2		2224.5	1578.8		
665.9	27(4)	0.25(11)	2093.8	1427.9		$(17/2^+)$
672.7	171(5)	0.33(6)	2135.7	1463.0	$(31/2^-)$	$25/2^+$
676.5	16(3)		2104.4+Δ	1427.9+Δ		$(21/2^+)$
687.1	392(8)	0.04(4)	686.9	0.0		$9/2^+$
704.5	6(2)[a]		2840.2	2135.7		$(31/2^-)$
730.9	10(2)[a]		2866.6	2135.7	$(33/2^+)$	$(31/2^-)$
759.1	16(3)[a]		2187.1+Δ	1427.9+Δ		$(21/2^+)$
791.0	12(3)		2218.9	1427.9		$(17/2^+)$
896.5	⩽ 2		2339.5	1443.4		
921.5	25(4)		4364.7	3443.2	$(37/2^-)$	$(37/2^+)$
925.4	18(3)		2353.3	1427.9		$(17/2^+)$

Table 2 — continued

E_γ	I_γ	A_2/A_0	E_i	E_f	J_i^π	J_f^π
1003.6	16(3)		2431.5	1427.9		$(17/2^+)$
1015.4	33(5)		2443.3+Δ	1427.9+Δ		$(21/2^+)$
1029.0	$\leqslant 2$		1715.9	686.9		
1050.9	142(6)	−0.04(8)	1050.8	0.0		$9/2^+$
1064.9	1000(26)	0.32(4)	1064.9	0.0	$15/2^-$	$9/2^+$
1110.8	23(2)		1796.9	686.9		
1122.0	180(16)	0.08(8)	1122.0	0.0	$7/2^+$	$9/2^+$
1160.6	70(3)		1160.6	0.0	$(9/2^+)$	$9/2^+$
1181.4	270(90)[a]		1181.4	0.0	$13/2^+$	$9/2^+$
1227.0	23(11)		2277.8	1050.8		
1257.1	$\leqslant 2$		1944.0	686.9		
1307.5	53(5)	0.41(10)	3443.2	2135.7	$(37/2^+)$	$(31/2^-)$
1409.2	60(5)		1409.4	0.0		$9/2^+$
1436.6	30(4)		1436.6	0.0		$9/2^+$
1469.3	6(2)[a]		4912.5	3443.2		$(37/2^+)$
1498.1	3(1)[a]		4364.7	2866.6	$(37/2^-)$	$(33/2^+)$

[a] Intensity deduced from coincidence spectra due to contamination in the singles.

3.2. *Transitions bypassing the τ_m = 36.4 s isomer*

This section discusses the placement of transitions shown in Fig. 2, which are not part of the yrast sequence and which bypass the α-decaying isomer, as observed in the ^{9}Be induced reaction.

The existence of a weak delayed component in the feeding of the $17/2^+$ level, with a mean life of 29(7) ns, was observed in the work of Fant et al. [5]. The isomeric level cannot be the 1428 keV level itself, as the major component of the 363.0 keV intensity is prompt with respect to the pulsed beam used in their experiment. (The lifetime of this level will be discussed in Section 3.4).

The present work confirms the existence of an isomeric state decaying to the 1428 keV level, as is clear from a comparison of the spectra which are prompt and early with respect to the 363.0 keV transition, shown in Figs. 4a and 4b, respectively. A clear division is established between transitions which feed the 1428 keV state through an isomeric level, and those bypassing it, populating the 1428 keV level directly. The most intense γ-ray in the 363.0 keV earlies spectrum is clearly the 308.1 keV transition, and the corresponding delayed spectrum for this line is shown in the lowest panel of this figure. Both transitions appearing in the delayed spectrum for the 308.1 keV γ-ray have been previously placed in the level scheme, and no candidates for a transition directly depopulating the isomer are obvious from the figure. It is likely that a highly converted (and hence unobserved), low-energy transition ($E_\gamma \leqslant 50$ keV) is responsible for the isomerism.

Finally, no coincidences between the 13 transitions directly populating the state at 1428 keV were found, resulting in the parallel placements shown in Fig. 2, and defining a large number of states in this energy region.

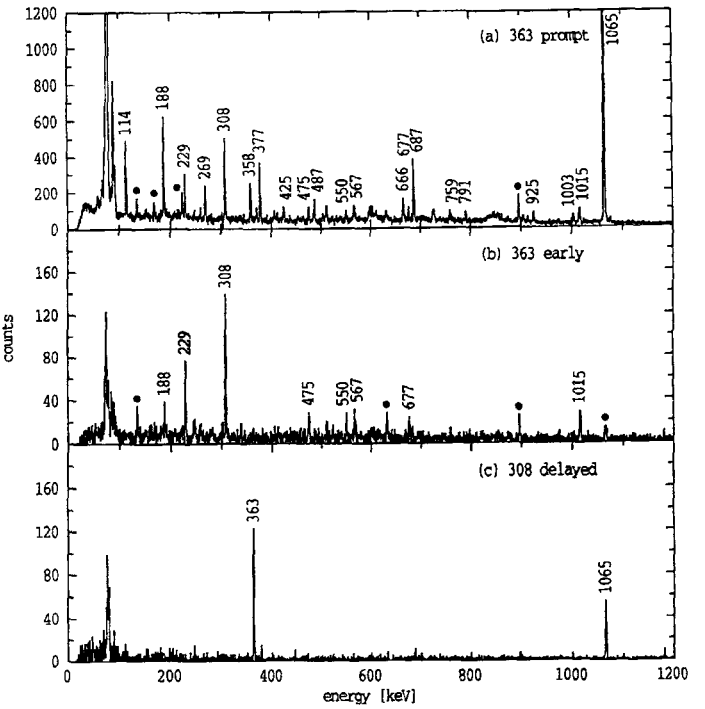

Fig. 4. (a,b) Prompt and early coincidence spectra gated by the 363 keV transition. (c) Delayed coincidence spectrum for the 308 keV transition. Contaminant transitions are indicated by the • symbol.

3.3. Transitions populating the $\tau_m = 36.4$ s isomer

The proposed yrast scheme above the $\tau_m = 36.4s$ isomer is shown in Fig. 2. All newly placed transitions in this scheme are in coincidence with polonium X-rays (see the inset of Fig. 5, for an example), are isolated from any previously known transitions in polonium isotopes and originate from mass 211 (as discussed in Section 3.1). Their placement and ordering are facilitated by the presence of two isomeric levels (the lifetimes of which are discussed in Section 3.4) which we have identified with the states at 2136 and 4873 keV, respectively.

The 672.7 keV transition, indicated in Fig. 1, is assigned as directly populating the isomer at 1463 keV. Coincidence relationships involving this transition are shown in Fig. 5. The uppermost spectrum in the figure originates from the ^{9}Be induced reaction, while the remaining spectra are from the ^{7}Li induced reaction. (The 672.7 keV gate taken in the latter reaction is heavily contaminated by the 676 keV γ-ray in ^{210}At.) It should also be noted that the spin input of the ^{7}Li induced reaction is somewhat higher than that of the ^{9}Be reaction (with semi-classical estimates of $27\hbar$ and $18\hbar$ respectively), hence coincidence spectra generated from the former reaction have been primarily used to establish the yrast scheme.

The assignment of the 672.7 keV γ-ray as populating the α-decaying isomer is deduced from the following considerations: the absence of delayed transitions in Fig. 5b

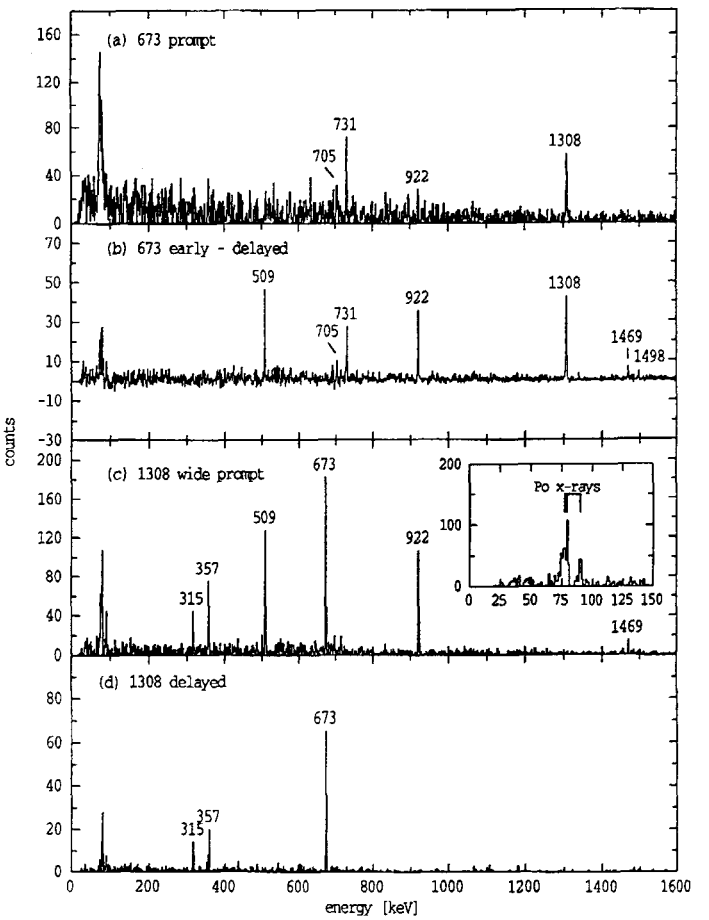

Fig. 5. (a,b) Prompt and early delayed coincidence spectra for the 673 keV transition. (c,d) Wide prompt and delayed spectra gated by the 1308 keV transition.

implies that the final state of the 672.7 keV transition is either the ground state or an excited state with a lifetime greater than several microseconds, while all transitions appearing in the 672.7 prompt (±120 ns) coincidence gate (as in Fig. 5a) must actually precede this transition in the decay scheme as they appear early in the 672.7 keV early delayed spectrum shown in Fig. 5b. The second possibility (that the 672.7 keV γ-ray populates the ground state) may be excluded, as the 672.7 keV transition would have been populated in the ^{208}Pb(α,n) reaction of [5], contrary to experiment. Assignment of the 672.7 keV transition as decaying to any state other than the α-decaying isomer requires the existence of a second low-lying isomer, with a long lifetime, for which there is no evidence or theoretical expectation. On this basis the existence of the state at 2136 keV is deduced. (Note that the excitation energies of all levels decaying to the α-decaying isomer are precisely determined up to the uncertainty of 6 keV in that of the isomer itself [10]).

The existence of an isomer populated by the 1307.5, 921.5 and 508.6 keV transitions

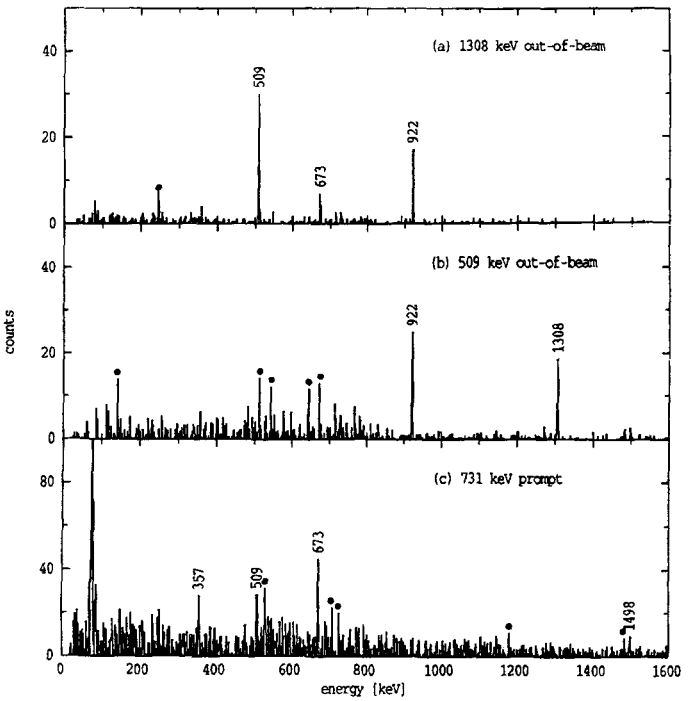

Fig. 6. (a,b) Out-of-beam spectra for the 1308 keV and 509 keV transitions. (c) Prompt coincidence spectrum for the 731 keV transition. Contaminant transitions are indicated by the • symbol.

and depopulated by the 672.7 keV transition is indicated by the presence of these transitions in the early-minus-delayed spectrum for the 672.7 keV γ-ray in Fig. 5b. This is confirmed by the delayed coincidence spectrum for the 1307.5 keV transition shown in the lowest panel of Fig. 5, which shows the 315.4 $\rightarrow$ 357.3 keV sequence in parallel with the 672.7 keV transition. The ordering of the 315.4 and 357.3 keV transitions was determined from their relative intensity in particle-gated singles spectra. The ordering amongst the 1307.5, 508.6 and 921.5 keV transitions shown in Fig. 2 is suggested from the relative (efficiency-corrected) intensities in the early-minus-delayed spectrum for the 672.7 keV transition (see Fig. 5), establishing the state at 3443 keV, depopulated by the 1307.5 keV γ-ray. The absence of the 508.6 keV transition from the upper panel of Fig. 5 is consistent with this ordering, given the lower spin input of the ^{9}Be induced reaction. These placements are also consistent with the 1307.5 keV wide prompt spectrum, shown in Fig. 5c, clearly displaying coincidences with the 508.6, 921.5 and 1469.3 keV transitions, while the parallel placements of the 704.5, 730.9 and 1498.1 keV are determined by their absence from this spectrum. The 730.9 prompt coincidence with the 1498.1 keV transition (see the lowest panel of Fig. 6) and the energy sum fixes the existence of the states at 2840, 2867 and 4913 keV.

Prompt, in-beam coincidence spectra for the 508.6 and 921.5 keV transitions are heavily contaminated by transitions of similar energy in ^{210}At in the ^{7}Li induced reaction, and are not available from the ^{208}Pb(^{9}Be,$\alpha 2n$) data due to the lower spin input in this

Table 3
Measured mean lives and transition strengths in ^{211}Po

Level Energy (keV)	J^π	E_γ (keV)	τ_m	γ_{BR} (%)	Mult	α_T	$B(QL)$ e^2 fm^{2L} or μ_n^2 fm^{2L-2}	$\lvert\mathcal{M}\rvert^2$ (s.p.u.)
1064.9	$15/2^-$	1064.9	20.2(3)[a]	95.6(2)	E3	0.015	$[55.7(8)]\times10^3$	19.1(3)
		377.6		4.4(2)	M2	0.914	20(3)	0.35(5)
1427.9+Δ	—	—	36(2)[b]	100	(E2)	—	—	—
2135.7	$(31/2^-)$	672.7	350(30)	90(1)	(E3)	0.047	$[65(7)]\times10^3$	0.11(2)
		315.4		10(1)	(M2)	1.64	6.8(6)	22.6(2)
3343.2	$(37/2^+)$	1307.5	$\leqslant 3$	100	(E3)	0.010	$\geqslant 88.3\times10^3$	$\geqslant 33.4$
4873.3	$(43/2^-)$	508.6	4000(1000)	100	(E3)	0.105	$[44(11)]\times10^3$	17(5)

[a] Previous measurements: 20(1) ns [5], 19.1(3) ns [6].
[b] Previous measurement: 29(7) ns [5].

reaction. These transitions can be isolated without contamination due to their delayed feeding from a second isomeric level, the existence of which is deduced from the upper panels of Fig. 6. Here, only transitions detected 200-800 ns after the beam pulse and in prompt coincidence with the 1307.5 keV line are shown. The assignment of the state at 4873 keV as isomeric is deduced from the presence of the 508.6, 672.7 and 921.5 keV transitions in this spectrum, and confirmed by that in Fig. 6b. Furthermore, the absence of the 1469.1 keV transition from Fig. 6a identifies the state at 4873 keV with the isomer rather than the state at 4913 keV. The lifetime of this isomer will be discussed in Section 3.4.

3.4. Lifetime measurements

Mean lives of excited states in ^{211}Po measured in this work are given in Table 3, together with those obtained in previous studies. Fig. 7 shows lifetime curves for three isomers, each generated using the γ–γ time difference method described in Section 2.3. The lifetime fits include convolution of the exponential decay curve with a Gaussian prompt response function. The lower panel of Fig. 8 shows the decay curve for the level at 4873 keV, obtained from γ-time data.

3.4.1. The isomer at 1064.9 keV

The decay curve of the $15/2^-$ state, obtained from time differences between the 363.0 and 1064.9 keV transitions, is shown in the lower panel of Fig. 7 together with a fit of 20.2(3) ns, in excellent agreement with the value of 20(1) ns obtained by Fant et al. [5].

3.4.2. The isomer at 1428+Δ keV

The middle panel of this figure displays the decay curve of the 1428+Δ keV isomer, intermediate to the decay of the 308.1 and 363.0 keV transitions. A mean life of 36(2) ns is obtained, a more precise value than that given in [5], but again in good agreement with that work.

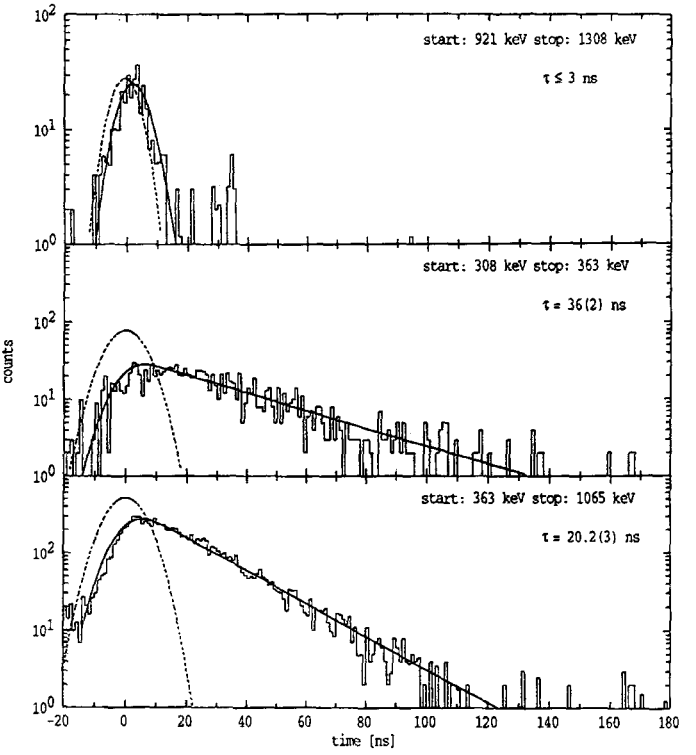

Fig. 7. Lifetime curves obtained from time differences for the 3343, 1428+Δ and 1065 keV levels, shown with fits of 3 ns, 36(2) ns and 20.2(3) ns respectively. A Gaussian with a FWHM identical to that included in the fit corresponding to a prompt decay ($\tau \leqslant 0.5$ ns) of the same intensity is shown superimposed at the time zero of each plot.

3.4.3. The 3443 keV level

The upper panel of Fig. 7 displays the decay curve for the 3443 keV level. (The position and width of the Gaussian prompt response function for this level have been extracted from a best fit to the time difference curve from the 1609 keV and 992 keV transitions in ^{209}Bi, where the intermediate $13/2^+$ state is known from Coulomb excitation studies [11] to have a lifetime less than 0.39 ns.) While the fit quality is insensitive to lifetimes of 0–2 ns, we place an upper limit of $\tau \leqslant 3$ ns on the lifetime of this state, as displayed in the figure.

3.4.4. The isomer at 2136 keV

The decay curve of the newly observed isomer at 2136 keV is given in the upper panel of Fig. 8, obtained as a sum of the time difference curves of the 1307.5, 921.5 and 508.6 keV transitions with respect to the 672.7 keV transition. A least squares fit to this curve yields a mean life of 350(30) ns.

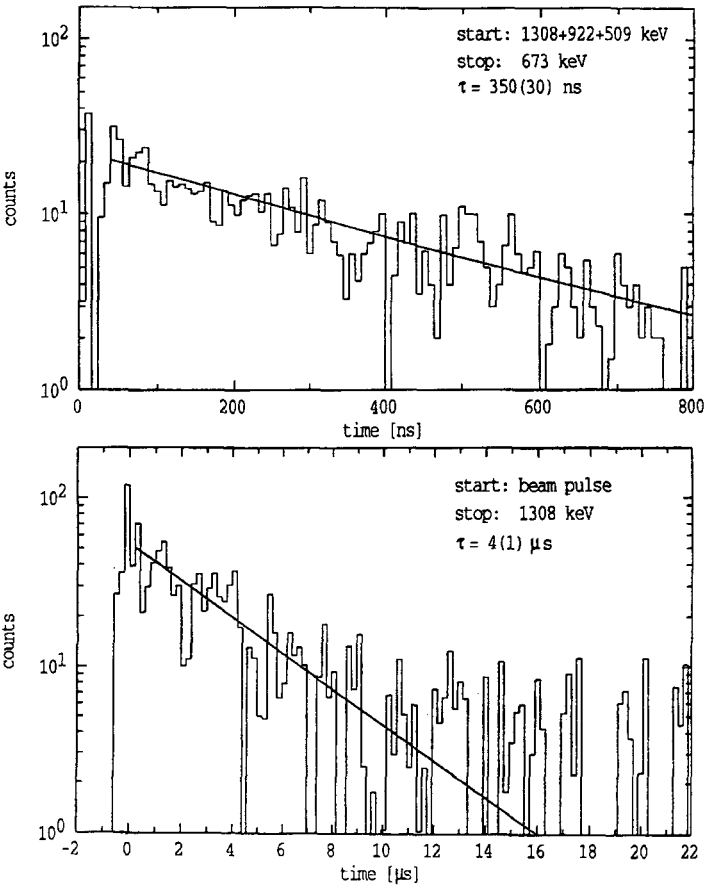

Fig. 8. Lifetime curves for the 2136 keV and 4873 keV levels, together with least-squares fits of 350(30) ns and 4(1) μs, respectively.

3.4.5. The isomer at 4873 keV

The time spectrum for the 1307.5 keV transition is shown in the lower panel of Fig. 8. Clean spectra for the 921.5 and 508.6 keV transitions were not available due to contamination from transitions in ^{210}At. Nonetheless, a value of 4(1) μs for the mean life of the isomer at 4873 keV is obtained, a value consistent with the presence of the 1307.5, 921.5 and 508.6 keV transitions in the 200–800 ns out-of-beam period.

3.5. Spin and parity assignments

Owing to the small yield of ^{211}Po in each of the reactions used and the large number of contaminant transitions present, direct measurement of conversion electron spectra was not practical. However, extraction of total conversion coefficients was possible for a few low-energy transitions through intensity balances. Anisotropies could be extracted for several transitions, as outlined in Section 2.2, where transitions were resolvable in the particle-gated singles spectrum. In such cases we have compared experimental a_2

values with theoretical values [12]. Where no spectroscopic information was available, in particular for the 921.5 and 508.6 keV transitions, we have adopted spins and parities suggested by the empirical shell-model calculations (see Section 4.1) as tentative assignments.

The 672.7 keV transition is adopted as $\lambda = 3$ as suggested by the observed a_2 coefficient of 0.33(6), while E3 is favoured over M3 on the basis of the measured lifetime of 350(30) ns for the initial state (the strength of an M3 assignment implies a reduced transition strength of 4 single-particle units (s.p.u.), too strong for such a transition in the trans-lead region). Hence the level at 2136 keV is assigned as $J^\pi = (31/2^-)$. The E3 assignment for the 672.7 keV transition, together with the observed relative γ-ray intensities of the 315.4 and 357.3 keV transitions when gated from above is consistent only with M2 and M1 assignments respectively to these latter two transitions. The use of theoretical total M1 conversion coefficient [13] of 0.334 for the 357.3 keV transition implies a total conversion coefficient of 2.4(9) for the 315.4 keV transition, consistent with the theoretical value of 1.64 for an M2 transition of this energy.

A value for the 1307.5 keV transition of $a_2 = 0.41(10)$ is obtained, hence $\lambda = 3$ has been adopted for this transition, while the upper limit for the lifetime of the state at 3443 keV ($\leqslant 3$ ns) favours E3 over M3. Hence we assign the state at 3443 keV as $J^\pi = (37/2^+)$.

The remaining levels in the proposed yrast sequence have spins and parities suggested from the shell-model calculations (see Section 4), while the reduced transition strengths implied by the lifetimes and multipolarities are summarised in Table 4.

4. Calculations and discussion

4.1. Empirical shell-model (ESM) calculations

The empirical shell-model approach, pioneered by Blomqvist and co-workers (of which Ref. [14] is an example) has been used with much success in the trans-lead region, and can be expected to provide reliable predictions, both of the structure and of the ordering of the yrast sequence, particularly in relatively simple systems such as ^{210}Po and ^{211}Po. We have performed empirical multi-particle shell model calculations for these nuclei, with the active proton orbitals being the $0h_{9/2}$, $1f_{7/2}$ and $0i_{13/2}$ orbitals and the $1g_{9/2}$, $0i_{11/2}$ and $0j_{15/2}$ as active neutron orbitals, including excitations across the $N = 126$ neutron shell gap, of which the $g_{9/2}p_{1/2}^{-1}$ particle–hole pair is likely to be the least energy-expensive. The calculations include a complete decomposition to two-body terms with diagonalisation of the resulting energy matrices. Two-body interaction energies are deduced from the spectra of nuclei close to the doubly-closed shell, except where empirical states are known to include significant configuration mixing, such as the semi-collective 5^- state in ^{208}Pb (with the $\nu(g_{9/2}p_{1/2}^{-1})$ configuration as the leading term [15]). In these cases, the empirical matrix elements display an apparent configuration dependence due to the effect of the Pauli principle; the presence of valence particles

Table 4
Nominal configurations in ^{211}Po. Energies are in keV

J^π	Level Energy	Calculated Energy	Assigned Configuration
$9/2^+$	0.0	48	$\pi(h)^2_{0^+}\nu g$
$11/2^+$	687.1	587	$\pi(h)^2_{0^+}\nu i$
$15/2^-$	1065	1079	$\pi(h)^2_{0^+}\nu j$
$13/2^+$	1181.4	1263	$\pi(h)^2_{2^+}\nu g$
$(17/2^+)$	1427.9	1477	$\pi(h)^2_{4^+}\nu g$
$(15/2^+)$	1458.6	1440	$\pi(h)^2_{4^+}\nu g$
$(21/2^+)$	1427.9+Δ	1516	$\pi(h)^2_{6^+}\nu g$
$(23/2^+)$		1649	$\pi(h)^2_{8^+}\nu g$
$(25/2^+)$	1463(6)	1530	$\pi(h)^2_{8^+}\nu g$
$(27/2^+)$	1820.3	1837.0	$\pi(h)^2_{8^+}\nu i$
$(31/2^-)$	2135.7	2105	$\pi(hi)_{11^-}\nu g$
$(33/2^+)$	2866.6	2850	$\pi(hi)_{11^-}\nu i$
$(37/2^+)$	3443.2	3408	$\pi(hi)_{11^-}\nu j$
$(33/2^-)$		4172	$\pi(h)^2_{8^+}\nu(g^2p^{-1})$
$(37/2^-)$	4364.7	4492	$\pi(h)^2_{8^+}\nu(gip^{-1})$
$(33/2^+)$		4465	$\pi(hf)_{8^+}\nu(g^2p^{-1})$
$(43/2^+)$	4873.3	4802	$\pi(hi)_{11^-}\nu(gip^{-1})$
$(39/2^+)$		4686	$\pi(hi)_{11^-}\nu(g^2p^{-1})$
$(37/2^{--})$		4370	$\pi(hf)_{8^+}\nu(gip^{-1})$
$(35/2^-)$		5102	$\pi(h)^2_{8^+}\nu(g^2f^{-1})$
$(47/2^-)$		5254	$\pi(hi)_{11^-}\nu(gjp^{-1})$
$(43/2^+)$		5359	$\pi(h)^2_{8^+}\nu(ijp^{-1})$

will block the presence of specific particle–hole components in the core excitation, the subsequent reduction in collectivity increasing the excitation energy of such a state when coupled to the valence particle configuration.

We have accounted for this dependence, in the case of the 5^- state in ^{208}Pb, by comparing the excitation energies of two multiparticle, high-spin isomers in ^{211}At and ^{212}At with spins and parities of $39/2^-$ and 19^+, respectively. Their configurations are believed [9] to differ by the presence of a $p^{-1}_{1/2}$ neutron hole, and it could be expected that the Pauli blocking is at least partly accounted for in these states. A simple weak-coupling estimate of the energy of the $39/2^-$ state compared to that of the 19^+ state then allows the extraction of a value of -117 keV for the $J = 5$, $\nu(g_{9/2}p^{-1}_{1/2})$ residual interaction, a 50% reduction in the magnitude of the matrix element obtained directly from the spectrum of ^{208}Pb. This value has then been used in all subsequent calculations. In addition, the recent work of Rejmund et al. [16] concerning high-spin states in ^{210}Pb allows the extraction of a value for the previously unknown $J = 10$, $\nu(g_{9/2}i_{11/2})$ interaction of -222 keV.

The results of the calculations are displayed in Fig. 9 together with the experimentally determined levels, while assigned configurations are summarised in Table 4.

The calculations for the known core-excited states of ^{210}Po are shown together with

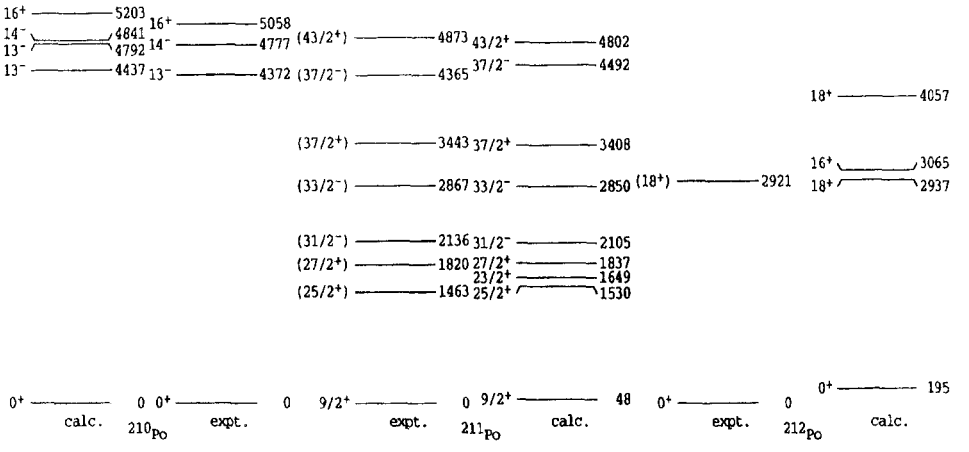

Fig. 9. Results of ESM calculations for ^{210}Po and ^{211}Po, together with the experimentally determined levels of each nucleus.

the full calculation for ^{211}Po. The yrast line of each nucleus is well produced, with most of the states shown predicted to be yrast by several hundred keV.

4.1.1. Seniority-three states decaying to the 1428 keV level

One feature of the proposed scheme requiring explanation is the high level density in the 1428–2500 keV excitation energy region. While no information on the multipolarity of these transitions is available from the measurements, they are likely to originate from the seniority-three states of the following configurations: $\pi((h_{9/2})^2_J \otimes \nu g_{9/2})$, $\pi((h_{9/2})^2_J \otimes \nu i_{11/2})$, $\pi((h_{9/2}f_{7/2})_J \otimes \nu g_{9/2})$ and $\pi((h_{9/2}f_{7/2})_J \otimes \nu i_{11/2})$ which together provide a total of 61 states with spins and parities between $15/2^+$ and $21/2^+$. The use of the excitation energies of the $h^2_{9/2}$ and $h_{9/2}f_{7/2}$ multiplets in ^{210}Po, (the properties of which have been extensively studied by Mann et al. [17]) and the excitation energy of the $11/2^-$ state in ^{211}Po of 687 keV leads to excitation energies for all the above configurations between 1200 keV and 3000 keV in ^{211}Po. Hence the high level density in ^{211}Po in this energy region appears to originate from the coupling of the $g_{9/2}$ and $i_{11/2}$ neutrons to the large number of two-proton states in the 1181–2438 keV energy region in ^{210}Po.

4.1.2. The 31/2$^-$, 27/2$^+$ and 25/2$^+$ levels

The most notable common structural feature of these isotopes is the similarity between the core-excited states of ^{210}Po and the $31/2^-$, $27/2^+$ and $25/2^+$ levels in ^{211}Po, in both the energy separations and the decay properties. Both the 16^+ and $31/2^-$ states decay through enhanced E3 transitions with reduced transition strengths of 19(1) [18] and 23(2) s.p.u. respectively, while the branching ratio for the decay is 94% for the former [19] and 90(1)% for the latter. The similar decay properties support the ESM interpretation for their structure as consisting of a $\pi(h_{9/2}i_{13/2}) \otimes \nu(g_{9/2})$ configuration in ^{211}Po coupled to a $\nu p^{-1}_{1/2}$ hole in ^{210}Po, with the final state of the decay arising

from the $J = 25/2^+$, $\pi(h_{9/2}^2) \otimes \nu(g_{9/2})$ configuration in ^{211}Po, again coupled to the $\nu p_{1/2}^{-1}$ hole in ^{210}Po. The hole can be envisioned as a 'spectator' with little influence on either the decay properties or the separation between the $\pi(h_{9/2}i_{13/2}) \otimes \nu(g_{9/2})$ and $\pi(h_{9/2}^2) \otimes \nu(g_{9/2})$ states.

4.2. Anomalous E3 reduced transition strengths

A feature requiring explanation is the magnitude of the E3 decay strength of both the 16^+ and $31/2^-$ states. The enhancement of E3 transitions over their single-particle estimates is a well-known feature of the decay of states in the trans-lead region, at least in those cases in which the single-particle orbitals involved in the transition differ by three units of angular momentum. In such cases, the single particle orbits are mixed through coupling to the octupole vibration of the ^{208}Pb core, enhancing the E3 transition strength through the occurrence of constructively interfering amplitudes in the initial and final wavefunctions and involving the $3^- \rightarrow 0^+$ transition of the core. However, the transitions are expected to be considerably less enhanced ($\leqslant 10$ s.p.u.) when the change in single-particle orbits is of a 'spin-flip' nature, ostensibly as the particle-vibration coupling is understood to act only on the spatial part of the single-particle wavefunctions [20]. The relevant single-particle transition in this case is the proton transition occurring in the decay of both the 16^+ and $31/2^-$ states:

$$|\tilde{i}_{13/2}\rangle \rightarrow |\tilde{h}_{9/2}\rangle,$$

where the tilde denotes the empirical state containing admixtures of octupole-coupled states, i.e.

$$|\tilde{i}_{13/2}\rangle = \alpha|i_{13/2}\rangle + \beta|f_{7/2} \otimes 3^-\rangle + \gamma|h_{9/2} \otimes 3^-\rangle$$

with a similar relation for the $|\tilde{h}_{9/2}\rangle$ state, specifically

$$|\tilde{h}_{9/2}\rangle = \delta|h_{9/2}\rangle + \epsilon|i_{13/2} \otimes 3^-\rangle.$$

However, the decays of the 16^+ and $31/2^-$ states, with transition strengths of 19(1) and 23(2) s.p.u. respectively, show an enhancement considerably larger than that expected for the spin-flip transition. Two possible explanations may resolve the discrepancy. The first is configuration mixing of the final states with the proton $|\tilde{h}_{9/2}\tilde{f}_{7/2}\rangle$ orbits, as suggested in [19]. Such an admixture in the final state permits the stronger $|f_{7/2} \otimes 3^-\rangle \rightarrow |f_{7/2}\rangle$ transition to proceed, which, when it occurs in the $11^- \rightarrow 8_2^+$, $|\tilde{h}_{9/2}\tilde{i}_{13/2}\rangle \rightarrow |\tilde{h}_{9/2}\tilde{f}_{7/2}\rangle$ decay transition in ^{210}Po, results in a strength of 20 s.p.u. [18]. The second possible explanation for the unexpectedly large transition strength implied by the decay of the 16^+ and $31/2^-$ isomers is that the particle-vibration matrix element, $\langle h_{9/2}|V_{PV}|i_{13/2} \otimes 3^-\rangle$, is underestimated due to the neglect of a possible spin dependence in the particle-vibration Hamiltonian, as discussed in [20]. An estimation of both the configuration mixing and the particle-vibration coupling requires a more complete calculation with the MPOC model [21–23], the subject of further work on this nucleus.

We have also proposed configurations for the $(37/2^-)$ and $(43/2^+)$ states which again involve the $|\tilde{h}^2_{9/2}\rangle$ and $|\tilde{h}_{9/2}\tilde{i}_{13/2}\rangle$ proton pairs, now coupled to the $|\tilde{g}_{9/2}\tilde{i}_{11/2}p^{-1}_{1/2}\rangle$ neutron configuration. While the spin and parity assignments must be regarded as tentative in this case, the implied transition strength of 19(5) s.p.u. is consistent with the decay properties of the proposed configuration. Presumably, the same mechanism(s) persist in the decay of the core-excited configurations; however, it should be noted that the proposed configuration of the $(43/2^+)$ state involves the $i_{11/2}$ neutron, the presence of which has been recently found [24] in ^{212}At to result in a 9% reduction of the octupole strength of the core through blocking of the $\nu(i_{11/2}f^{-1}_{5/2})$ particle–hole component of the 3^- vibration. To what degree such an effect will compete with the anomalous $|\tilde{i}_{13/2}\rangle \rightarrow |\tilde{h}_{9/2}\rangle$ transition strength is not clear, and clearly a decisive lifetime measurement for the $(43/2^+)$ state is required.

4.3. *Implications for $^{212}Po^m$*

Our assignment of $J^\pi = 37/2^-$ for the state at 4365 keV, arising from the $\pi(h^2_{9/2}) \otimes \nu(g_{9/2}i_{11/2}p^{-1}_{1/2})$ configuration, has clear implications for the structure of the $J^\pi = (18^+)$, $\tau_m = 65$ s α-decaying isomer in ^{212}Po [22]. Configurations possible for this isomer are (see Ref. [23] and references therein)

$$J = 18^+, \qquad \pi(h^2_{9/2})_8 \otimes \nu(g_{9/2}i_{11/2})_{10}, \tag{1}$$

$$J = 18^+, \qquad \pi(h^2_{9/2})_8 \otimes \nu(i^2_{11/2})_{10}, \tag{2}$$

$$J = 16^+, \qquad \pi(h^2_{9/2})_8 \otimes \nu(g^2_{9/2})_8. \tag{3}$$

Whichever configuration is that of the (18^+) isomer, the residual interactions responsible for its low excitation energy are present regardless of the $p^{-1}_{1/2}$ neutron hole, so that the corresponding state should be the most energetically favoured core excited state in ^{211}Po. The ESM calculations yield an excitation energy of 4057 keV for configuration (2), more than 1 MeV greater than the observed value for the isomer. Given the accuracy of the calculations of 50 keV or less for high-spin states in ^{210}Po and ^{211}Po, this configuration seems unlikely.

We may reasonably expect the observed core-excited sequence in ^{211}Po to be related simply to the highest-spin valence states below the core-excited region ^{212}Po, in a manner analogous to the relationship between the 16^+ and $31/2^-$ states ^{210}Po and ^{211}Po. While we calculate an excitation energy of 3065 keV for configuration (3), the observation that no state of spin 33/2 competes to form the lowest energy, core-excited state in ^{211}Po is systematic evidence excluding spin 16 as that of the $\tau_m = 65$ s isomer in ^{212}Po. However, this inference relies on the accuracy of the spin assignments proposed in this work, which are tentative for the level at 4365 keV.

The lowest assigned core-excited state in this nucleus is the $J^\pi = (37/2^-)$ state at 4365 keV. From the energy of this state, one can make a weak-coupling estimate of the energy of a corresponding 18^+ state in ^{212}Po obtained by removal of the $p^{-1}_{1/2}$ neutron

hole. If ΔV is the difference in the total residual interaction energies between the 18^+ and $37/2^-$ configurations due to the absence of the neutron hole, then the excitation energy of the 18^+ state is obtained from that of the $37/2^-$ state via

$$E_{ex}(18^+) = E_{ex}(37/2^-) - \epsilon(p_{1/2}^{-1}) + M(^{211}\mathrm{Po}) - M(^{212}\mathrm{Po}) + \Delta V \quad (4)$$

and hence, with the adopted value of -117 keV for the $g_{9/2}p_{1/2}^{-1}$ interaction, this yields

$$E_{ex}(18^+) = 4365 - 7368 - 13334 + 19343 + (117 - 190 + 4) = 2937 \text{ keV}, \quad (5)$$

while the experimentally determined energy of the 18^+ isomer is 2921(15) keV. Hence, while the spin and parity assignment for the level at 4365 keV is tentative, the assigned configuration for this state in ^{211}Po is consistent with that of Poletti et al. [25] in ^{212}Po, who favour a $\pi(h_{9/2}^2) \otimes \nu(g_{9/2}i_{11/2})$ assignment for the configuration of the $\tau_m = 65$ s isomer.

4.4. Conclusion

High spin states in ^{211}Po have been populated through incomplete fusion reactions, and their subsequent decay studied by in-beam γ-ray spectroscopy. As a result of this study, the yrast structure of ^{211}Po has been extended to $J^\pi = (43/2)^+$ at 4873 keV. The yrast states decaying to the α-decaying, $\tau_m = 36.4$ s isomer display similar decay properties to the known core-excited states in ^{210}Po, supporting their shell-model interpretation as differing only by presence of a $p_{1/2}^{-1}$ neutron hole in ^{210}Po. In addition, the excitation energy of the $\pi(h_{9/2}^2)\otimes\nu(g_{9/2}i_{11/2}p_{1/2}^{-1})$ configuration for the $J^\pi = (37/2^-)$ core-excited state is consistent with $J^\pi = 18^+$ for the $\tau_m = 65$ s isomer in ^{212}Po, the configurations again differing only by the absence of the $p_{1/2}^{-1}$ neutron hole in the heavier isotope.

Acknowledgements

The authors would like to thank the technical staff of the ANU Heavy-Ion Facility for their assistance over the course of these studies.

References

[1] S.M. Mullins, G.D. Dracoulis, A.P. Byrne, T.R. McGoram, S. Bayer, W.A. Seale and F.G. Kondev, Phys. Lett. B 393 (1997) 279.
[2] G.D. Dracoulis, A.P. Byrne, T. Kibédi, T.R. McGoram and S.M. Mullins, Proceedings of the FUSION 97 Conference', J. Phys. G: Nucl. Part. Phys. 23 (1997) 1191.
[3] W.J. Kox, A.R. Quinton and C.E. Anderson, Phys. Rev. 120 (1960) 2120.
[4] M. Dasgupta, private communication.
[5] B. Fant, T. Lönnroth and V. Rahkonen, Nucl. Phys. A 355 1981 171.
[6] T. Faestermann, F. Feilitzsch, K.E.G. Löbner, C. Signori, T. Yamazaki, C.V.K. Baba and D.B. Fossan, Proc. Int. Conf. On Nuclear Moments and Nuclear Structure, Osaka 1972, ed. H. Horie and K. Sugimoto, Phys. Soc. Japan Suppl. 34 (1973) 287.

[7] G.D. Dracoulis and A.P. Byrne, ANU-P/1052 (1989) 115, unpublished.
[8] G.J. Lane, A.P. Byrne and G.D. Dracoulis, Department of Nuclear Physics, Annual Report ANU-P/1118 (1992) p. 114, unpublished.
[9] S. Bayer, Australian National University PhD thesis (1998), unpublished;
S. Bayer et al., to be published.
[10] M.J. Martin, Nucl. Data Sheets 25 (1978) 397; 27 (1979) 637.
[11] J.W. Hertel, D.G. Fleming, J.P.Schiffer and H.E. Gove, Phys. Rev. Lett. 23 (1969) 488.
[12] E. der Mateosian and A.W. Sunyar, Atomic Data and Nucl. Data Tables 11 (1974) 407.
[13] F. Rössel, H.M. Fries, K. Alder and H.C. Pauli, Atomic Data and Nucl. Data Tables 21 (1978).
[14] V. Rahkonen, I. Bergström, J. Blomqvist, O. Knuuttila, K.-G. Rensfelt, J. Sztarkier and K. Westerberg, Z. Phys. A 284 (1978) 357.
[15] P. Ring and J. Speth, Nucl. Phys. A 235 (1974) 315.
[16] M. Rejmund, K.H. Maier, R. Broda, M. Lach, J. Wrzesinski, J. Agramunt, J. Blomqvist, A. Gadea, J. Gerl, M. Gorska, H. Grawe, M. Kaspar, I. Kozhoukharov, I. Peter, H. Schaffner, R. Schubart, Ch. Schlegelm, G. Stengel, S. Wan, H.J. Wollersheim, Z. Phys. A 359 (1997) 243.
[17] L.G. Mann, K.H. Maier, A. Aprahamian, J.A. Becker, D.J. Decman, E.A. Henry, R.A. Meyer, N. Roy, W. Stöffl and G.L. Struble, Phys. Rev. C 38 (1988) 74.
[18] B. Fant, Physica Scripta 4 (1971) 175.
[19] I. Bergström, J. Blomqvist, P. Carlé, B. Fant, A. Källberg, L.O. Norlin, K.-G. Rensfelt and U. Rosengård, Physica Scripta 31 (1985) 333.
[20] I. Hamamoto, Phys. Rep. 10 (1974) 63.
[21] G.D. Dracoulis, C.A. Steed, A.P. Byrne, S.J. Poletti, A.E. Stuchbery and R.A. Bark, Nucl. Phys. A 462 (1987) 576.
[22] G.D. Dracoulis, Structure of high-spin isomers in trans-lead nuclei, Proceedings of the XXV Zakopane School of Physics (1990).
[23] A.E. Stuchbery, G.D. Dracoulis, A.P. Byrne, S.J. Poletti and A.R. Poletti, Nucl. Phys. A 482 (1988) 692.
[24] A.P. Byrne, S. Bayer, G.D. Dracoulis and T. Kibédi, Phys. Rev. Lett. 80 10 (1998) 2077.
[25] A.R. Poletti, G.D. Dracoulis, A.P. Byrne and A.E. Stuchbery, Nucl. Phys. A 473 (1987) 595.
[26] I. Perlman et al., Phys. Rev. 127 (1962) 917.